JACS
JOURNAL OF THE AMERICAN CHEMICAL SOCIETY
Communication
pubs.acs.org/JACS

Monodisperse and Inorganically Capped Sn and Sn/SnO_2 Nanocrystals for High-Performance Li-Ion Battery Anodes

Kostiantyn Kravchyk,[†,‡] Loredana Protesescu,[†,‡] Maryna I. Bodnarchuk,[†,‡] Frank Krumeich,[†] Maksym Yarema,[†,‡] Marc Walter,[†] Christoph Guntlin,[†] and Maksym V. Kovalenko*[,†,‡]

[†]Institute of Inorganic Chemistry, Department of Chemistry and Applied Biosciences, ETH Zürich, CH-8093 Zürich, Switzerland
[‡]EMPA-Swiss Federal Laboratories for Materials Science and Technology, CH-8060 Dübendorf, Switzerland

Supporting Information

ABSTRACT: We report a facile synthesis of highly monodisperse colloidal Sn and Sn/SnO_2 nanocrystals with mean sizes tunable over the range 9−23 nm and size distributions below 10%. For testing the utility of Sn/SnO_2 nanocrystals as an active anode material in Li-ion batteries, a simple ligand-exchange procedure using inorganic capping ligands was applied to facilitate electronic connectivity within the components of the nanocrystalline electrode. Electrochemical measurements demonstrated that 10 nm Sn/SnO_2 nanocrystals enable high Li insertion/removal cycling stability, in striking contrast to commercial 100−150 nm powders of Sn and SnO_2. In particular, reversible Li-storage capacities above 700 mA h g^{-1} were obtained after 100 cycles of deep charging (0.005−2 V) at a relatively high current of 1000 mA h g^{-1}.

Tin is a nontoxic, inexpensive, and naturally highly abundant element that is among the most technologically important metals. For instance, it is used not only as corrosion-resistant plating of food cans and in metal alloys such as bronze and solder but also in emerging photovoltaic materials such as Cu−Zn−Sn chalcogenides and next-generation rechargeable Li-ion batteries (LIBs). In this work, we were driven by two goals: (i) to develop a robust synthesis of monodisperse Sn nanocrystals (NCs) and (ii) to study the size-dependent cycling performance of nanocrystalline Sn-based LIB anodes. For the latter, finely tunable morphologies and optimal surface chemistries in the sub-50 nm size range are considered crucial for achieving high charge/discharge cycling stabilities in the next-generation high-capacity anode materials based on Li alloys with Si, Sn, and Ge.[1] Furthermore, the potential use of Sn and the corresponding oxide SnO_2 in a monodisperse colloidal state is broader by far, including solution-deposited transparent conductive oxides for electronics, photovoltaics, and sensors as well as quantum dots (sub-5 nm α-Sn)[2] or low-temperature catalysts for growing nanowires.[1b] In addition, quantum-size effects in Sn nanoparticles (NPs) have been demonstrated to modify their superconducting properties at cryogenic temperatures.[3]

Despite numerous reports on rather polydisperse [size deviation (σ) >15%] and/or relatively large (30−200 nm) and nonuniform Sn colloids,[4] the robust synthesis of monodisperse sub-30 nm Sn NCs has remained undeveloped. The low melting point of bulk Sn (231.9 °C) requires the synthesis to be carried out at sufficiently low temperatures using either highly reactive precursors or strong reducing agents. Our new approach to monodisperse Sn NCs was inspired by recent successes in using metal amides as precursors for monodisperse colloids, including metallic Bi,[5] Pb,[6] In,[7] Co,[8] Fe,[9] FeRh,[10] and FeCo[11] NCs and NCs of compounds such as SnTe,[12] PbSe, and Ag_2Se.[13]

Monodisperse 9−23 nm Sn NCs [Figure 1; for details, see the Supporting Information (SI), including Table S1] were obtained by injection of $LiN(SiMe_3)_2$ into a hot oleylamine (OLA) solution containing $SnCl_2$ or $Sn[N(SiMe_3)_2]_2$ at 180−210 °C followed by reduction with diisobutylaluminium hydride (DIBAH). Inexpensive $SnCl_2$ and $LiN(SiMe_3)_2$ were used as initial precursors because of the possibility of forming of $Sn[N(SiMe_3)_2]_2$ in situ. Instead, ^{119}Sn NMR spectra taken at various stages of the synthesis (Figures 2 and S1) showed that in situ- or ex situ-prepared $Sn[N(SiMe_3)_2]_2$ is not an actual precursor. A different reaction mechanism is plausible: fast in situ formation of metal−oleylamide species. An important role of $LiN(SiMe_3)_2$ is to act as a base to deprotonate OLA. Formation of lithium oleylamide is facilitated by the volatility of $HNSiMe_3$, and it quickly reacts with $SnCl_2$ to generate a Sn−oleylamido complex, the actual precursor for the final reduction step. Very similar results, judging from ^{119}Sn NMR spectra, reaction rates, and the size and shape uniformity of the Sn NCs, were obtained using sodium and potassium silylamides, other strong bases such as LiH and $LiNMe_2$ (Figure S2), and various OLA-soluble Sn(II) precursors such as $Sn[N(SiMe_3)_2]_2$, $Sn(Ac)_2$, and $Sn(CF_3SO_3)_2$ (Figure S3). In agreement with the proposed role of organic bases, no NCs were formed in their absence; only polydisperse 100−300 nm Sn particles were collected after injection of DIBAH directly into Sn(II) salts in OLA (Figure S4). Very likely Sn−oleylamido complexes and/or lithium oleylamide may act as not only a precursor but also a surface-capping layer during NC nucleation and growth (rather than neutral OLA molecules). These observations may also explain the "magic role" of excess $LiN(SiMe_3)_2$ in the recent preparations of Bi,[5] In,[7] Ag_2Se, CdSe, and PbSe NCs.[13] Further mechanistic studies on the in situ formation of metal/long-chain amide complexes for the NC synthesis are underway and will be reported elsewhere.

The isolation and purification of Sn NCs was carried out in air. Oleic acid was added to replace weakly bound oleylamide/OLA species (Figure S5). High-resolution bright-field scanning transmission electron microscopy (BF-STEM) and high-angle

Received: December 26, 2012
Published: February 15, 2013

   dx.doi.org/10.1021/ja312604r | J. Am. Chem. Soc. 2013, 135, 4199−4202

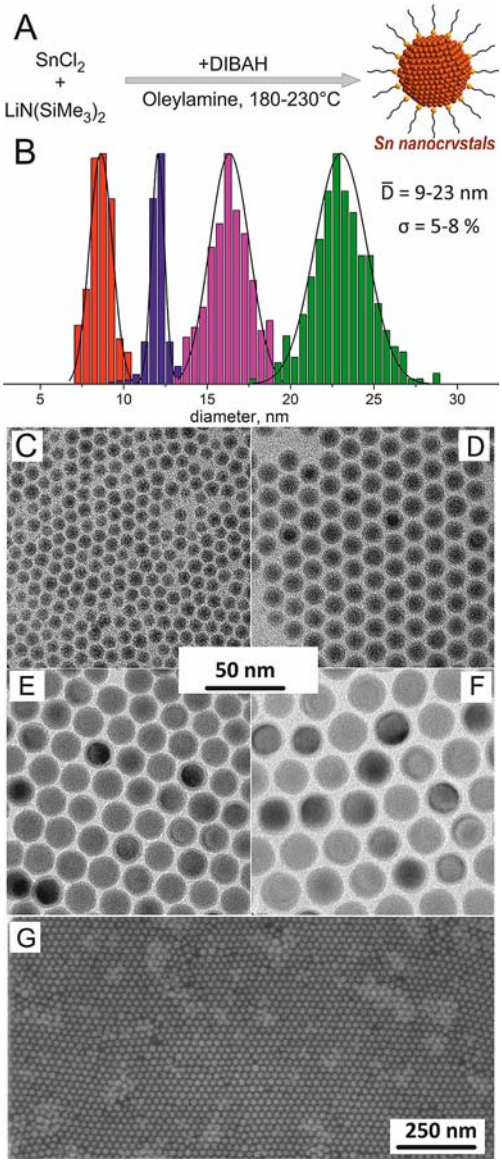

Figure 1. (A) Synthesis of monodisperse Sn NCs. (B) Size histograms ($\sigma \approx 8.3$, 5.9, 7.7, and 7.6% for 9, 12, 16, and 23 nm NCs, respectively). (C–F) Corresponding TEM images. (G) SEM image of 16 nm NCs.

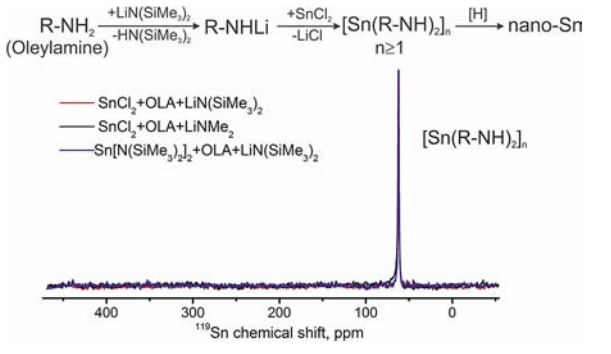

Figure 2. Proposed mechanism of precursors-to-metallic Sn conversion (top) derived from NMR studies in OLA (bottom). Regardless of the Sn(II) counterion (Cl^-, AcO^-, TfO^-, or silylamide), addition of $LiNMe_2$ or $LiN(SiMe_3)_2$ leads to the same Sn–oleylamido derivatives.

annular dark-field STEM (HAADF-STEM) images of Sn NCs (Figure 3A,B) indicated a single-crystalline core covered by an

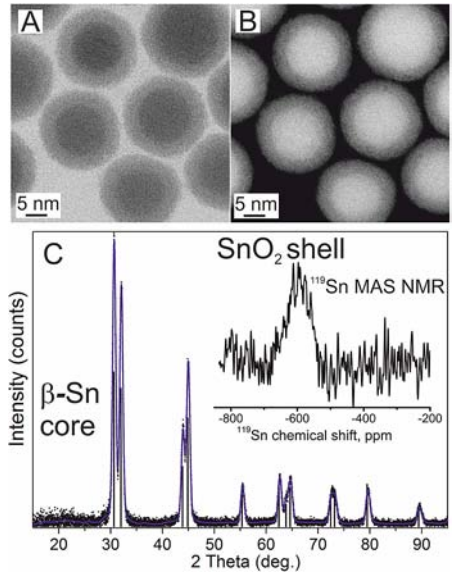

Figure 3. (A) BF-STEM image, (B) HAADF-STEM image, and (C) PXRD pattern and (inset) ^{119}Sn MAS NMR spectrum of colloidal Sn/SnO_2 NCs. Vertical lines in (C) mark the diffraction pattern of bulk β-Sn; the blue curve is the fit obtained by Rietveld refinement.

amorphous oxide shell formed upon exposure to air. The oxide thickness of 2–3 nm was retained after the samples were stored in air for 6 months. Powder X-ray diffraction (PXRD) patterns (Figures 3C and S6) confirmed that NC cores were single-crystalline β-Sn (space group $I41/amd$; $a = 0.58308$, $c = 0.31810$ nm)[14] without detectable crystalline tin oxide phases. Magic-angle-spinning (MAS) ^{119}Sn NMR spectra of powdered samples contained a single broad peak at ca. −600 ppm, as commonly reported for amorphous SnO_2, and no signs of SnO (expected at −208 ppm) were observed.[15] The peak broadening of up to 100 ppm was similar to those reported for sub-10 nm SnO_2 NPs and hollow SnO_2 nanospheres,[16] while much narrower peaks (<10 ppm) were found in bulk crystalline SnO_2.[15]

As expected, the highly insulating oleate capping layer makes the Sn NCs unusable as a Li-ion storage material, leading to negligible discharge capacities of ∼20 mA h g^{-1}. We therefore employed an inorganic capping approach in which oleate ligands were displaced with smaller inorganic ions such as SH^- and S^{2-} in a phase-transfer ligand-exchange reaction.[17] Sn NCs dispersed in hexane or tetrachloroethylene were treated with KHS solution in formamide (FA), which led to fast and complete migration of NCs into the polar FA phase. Subsequently, the NCs were precipitated with MeCN and redispersed in water, forming concentrated and stable colloidal solutions (Figure 4A). Importantly, the size and shape of the NCs were retained upon ligand exchange (Figure 4B), while the mechanism of colloidal stabilization changed from steric to electrostatic repulsion. Strong negative surface charge due to surface-bound inorganic ions was evident from measurements of the electrophoretic mobility (Figure 4C). Dynamic light scattering (DLS) measurements confirmed that HS^-/SO_4^{2-}-capped Sn/SnO_2 NCs possessed true colloidal stability with a monomodal size dispersion (Figure S7). The complete removal of organic ligands was also apparent from the lack of absorption in the 2800–3000 cm^{-1} region (CH vibrations). Instead, attenuated total reflection (ATR) FTIR spectra indicated a large number of SO_4^{2-} ions. Two major absorption bands, assigned to the ν_3 (1110 cm^{-1}) and ν_4 (618 cm^{-1}) vibrations of SO_4^{2-},[18] were found for both the

dx.doi.org/10.1021/ja312604r | J. Am. Chem. Soc. 2013, 135, 4199–4202

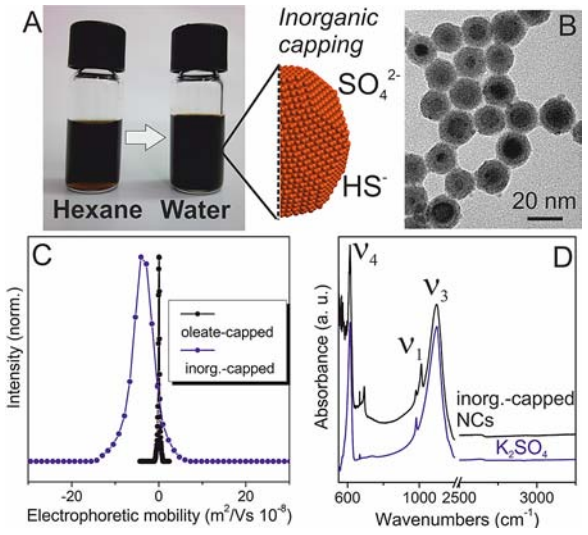

Figure 4. (A) Photograph illustrating phase transfer of Sn/SnO_2 NCs from hexane into water induced by the ligand-exchange reaction and (B) corresponding TEM image, (C) electrophoretic mobility, and (D) ATR-FTIR spectra of HS^-/SO_4^{2-}-functionalized Sn/SnO_2 NCs.

NCs and the reference, K_2SO_4. The weak ν_1 band (982 cm^{-1}) was also found in both spectra. The frequency of ν_1 is known to be variable in the 980−1020 cm^{-1} range, often without considerable shifts of ν_3 and ν_4.[18b] Hence, the weak absorption line at 1010 cm^{-1} may be attributed to the ν_1 band of surface-bound SO_4^{2-}. The large amounts of SO_4^{2-} may be attributed to partial oxidation of S^{2-}.

The widespread use of group-IV elements as anode materials in LIBs is mainly hindered by the mechanical instabilities and pulverization of electrodes caused by the large (up to 300%) volumetric changes upon full lithiation to Sn_5Li_{22} (corresponding to a theoretical capacity of 992 mA h g^{-1}).[19] Downsizing the active material to a nanosized morphology can help mitigate these difficulties.[1a,c−e] In the case of Sn/SnO_2, the contribution of SnO_2 may reduce the achievable reversible capacity to that of pure SnO_2 (780 mA h g^{-1}) because of the first-discharge irreversible reaction $SnO_2 + 4Li \rightarrow 2Li_2O + Sn$. However, the resulting thin Li_2O shell may help buffer the volume changes and reduce the tendency to sinter. For a closely related case of Si NPs, Tarascon and co-workers showed that simple mixing of the active material with large quantity of amorphous carbon, commonly used as an elastic and conductive matrix, can significantly improve the cycling stability if the gravimetric fraction of the active Si material does not exceed 20−30%.[1d] Thus, our initial electrochemical studies (Figure 5A−C) were carried out using a traditional formulation for the electrodes, namely, a mixture of NCs with amorphous carbon and polymer binder in a gravimetric ratio of 30% NCs/45% carbon/25% binder. Anodes for standard coin-type Li-ion cells (using metallic Li as a counter electrode; for details, see the SI) were deposited from colloidally stable aqueous dispersions of Sn/SnO_2 NCs mixed with carbon black and with sodium carboxymethylcellulose (CMC) as a water-soluble binder.[20]

Test cells were cycled over the range 0.005−2 V, which can be considered as deep charging/discharging, and the obtained capacities were normalized by the mass of Sn-containing nanomaterial. It should be noted that any narrower voltage range would give substantially higher capacity retention upon cycling. Furthermore, we used relatively high charge/discharge rates of 1000 mA/g (1−2 C depending on the capacity), similar to those required for applications of LIBs in electrical vehicles and portable electronics. Contrary to organic capping, fully inorganic NCs exhibited high reversible discharge capacities of up to C_{Sn}^{max} = 1000 mA h g^{-1} for the cells containing 30 wt % Sn (Figure 5A,C). We designate this value as an upper estimate, as the possible contribution from the carbon matrix was neglected.

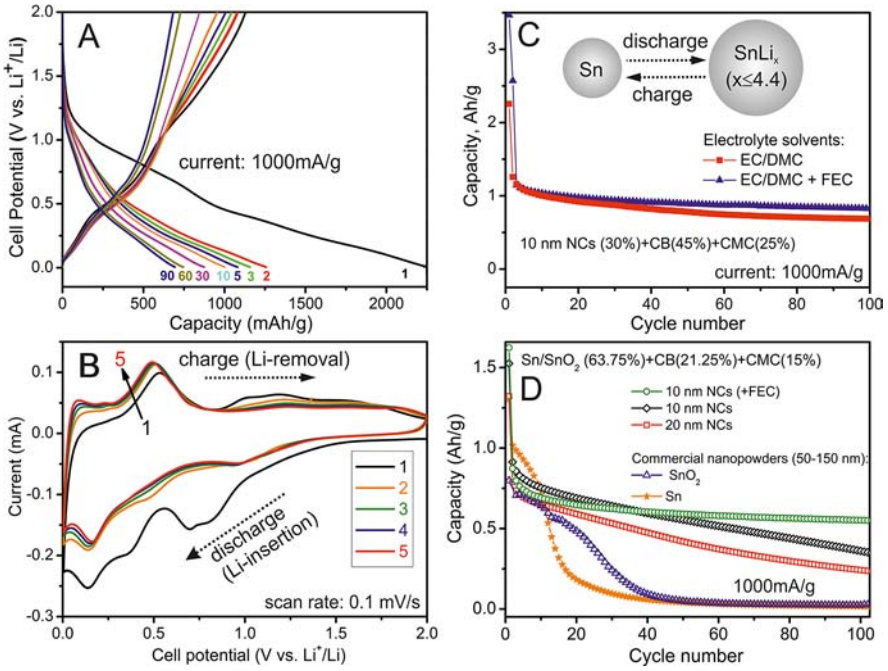

Figure 5. (A) Galvanostatic discharge profiles for anodes containing 10 nm Sn/SnO_2 NCs. (B) CVs for the initial five charge−discharge cycles for electrodes containing 10 nm Sn/SnO_2 NCs (scan rate = 0.1 V/s). (C, D) Reversible discharge capacities (normalized by the content of active material) for anodes containing (C) 30 wt % Sn/SnO_2 NCs and (D) a high mass content (63.75%) of an active Sn-based material (NCs or commercial powders).

dx.doi.org/10.1021/ja312604r | J. Am. Chem. Soc. 2013, 135, 4199−4202

The most conservative estimate, C_{Sn}^{min} = 700 mA h g^{-1}, was obtained by assuming that the capacity of ~200 mA h g^{-1} for carbon (measured separately under identical conditions) was retained in the mixture with NCs. Cyclic voltammograms (CVs) (Figure 5C) were fully consistent with the earlier reports for nano- and microgranular SnO_2[19,21] and Sn.[22] During the first discharge, we observed a cascade of reduction waves corresponding to (from higher to lower potential) reduction of SnO_2 to Sn, formation of the solid−electrolyte interface, and alloying of Sn with Li. The reduction peaks at 0.25−0.7 V are due to the formation of Li_2Sn_5, LiSn, Li_7Sn_3, Li_5Sn_2, $Li_{13}Sn_5$, Li_7Sn_2, and $Li_{22}Sn_5$.[19] The broad peak at 0.5 V in the positive current range (charging) includes all of the dealloying steps. For better long-term cycling stability, fluoroethylene carbonate (FEC)[23] was added to the electrolyte, leading to the retention of 85−90% of the 20 s cycle capacity after 100 cycles (Figure 5B).

Comparisons of the basic electrochemical data such as reversible capacities and their retention in numerous reports may be misleading and must be viewed with caution. Unambiguous and practically meaningful comparisons can be made only for test electrodes containing the same volume or mass fraction of active material, having similar electrode densities and thicknesses, and studied under identical electrochemical conditions (i.e., voltage window, charge/discharge current, temperature, and electrolyte composition). With this in mind, we investigated the importance of precisely engineered NC sizes for improving the Li insertion properties. Figure 5D compares electrodes containing 10 nm and 20 nm Sn/SnO_2 NCs with those employing commercial Sn and SnO_2 nanopowders (Aldrich, 50−150 nm; Figures S8 and S9). Furthermore, to have more practical formulations of electrodes, we increased the content of the active Sn material to ~64 wt %. Under these conditions, after 100 cycles, only large (10 nm) Sn/SnO_2 NCs could retain capacities of C_{Sn}^{max} = 600 mA h g^{-1} and C_{Sn}^{min} = 443 mA h g^{-1} (electrode density of ~2 g/cm^3). These preliminary data compare very favorably with the theoretical capacity of 372 mA h g^{-1} for graphite, a major consistuent of commercial anodes. Notably, the commercial Sn and SnO_2 nanopowders initially showed similar capacities, but these quickly faded within the first 50 cycles.

In summary, we have reported a simple colloidal synthesis that allows highly monodisperse Sn and Sn/SnO_2 NCs with sizes of 9−23 nm to be grown. We have also shown that after proper surface functionalization, these NCs exhibit stable Li-ion insertion properties with capacities close to the theoretical value. Furthermore, under a high mass load of the active material, the smallest tested NCs (~10 nm) exhibited much higher charge/discharge cycling stabilities than commercial nanopowders with large sizes of 50−150 nm. Colloidal Sn NCs may also be useful as a low-melting-point catalyst for growing one-dimensional Si and Ge nanostructures.

■ ASSOCIATED CONTENT

Supporting Information

Experimental details and supporting figures. This material is available free of charge via the Internet at http://pubs.acs.org.

■ AUTHOR INFORMATION

Corresponding Author

mvkovalenko@ethz.ch

Notes

The authors declare no competing financial interest.

■ ACKNOWLEDGMENTS

This work was financially supported by the Swiss National Science Foundation (SNF, Project 200021_140245) and ETH Zürich. Electron microscopy was performed at the ETH Zürich Electron Microscopy Center and the EMPA Electron Microscopy Center.

■ REFERENCES

(1) (a) Magasinski, A.; Dixon, P.; Hertzberg, B.; Kvit, A.; Ayala, J.; Yushin, G. *Nat. Mater.* **2010**, *9*, 353. (b) Chockla, A. M.; Klavetter, K. C.; Mullins, C. B.; Korgel, B. A. *Chem. Mater.* **2012**, *24*, 3738. (c) Kovalenko, I.; Zdyrko, B.; Magasinski, A.; Hertzberg, B.; Milicev, Z.; Burtovyy, R.; Luzinov, I.; Yushin, G. *Science* **2011**, *333*, 75. (d) Beattie, S. D.; Larcher, D.; Morcrette, M.; Simon, B.; Tarascon, J. M. *J. Electrochem. Soc.* **2008**, *155*, A158. (e) Chan, C. K.; Peng, H.; Liu, G.; McIlwrath, K.; Zhang, X. F.; Huggins, R. A.; Cui, Y. *Nat. Nanotechnol.* **2008**, *3*, 31.

(2) Allan, G.; Delerue, C. *ACS Nano* **2011**, *5*, 7318.

(3) Bose, S.; Garcia-Garcia, A. M.; Ugeda, M. M.; Urbina, J. D.; Michaelis, C. H.; Brihuega, I.; Kern, K. *Nat. Mater.* **2010**, *9*, 550.

(4) (a) Yang, C.-S.; Liu, Q.; Kauzlarich, S. M.; Phillips, B. *Chem. Mater.* **2000**, *12*, 983. (b) Nayral, C.; Ould-Ely, T.; Maisonnat, A.; Chaudret, B.; Fau, P.; Lescouzères, L.; Peyre-Lavigne, A. *Adv. Mater.* **1999**, *11*, 61. (c) Wang, X.-L.; Feygenson, M.; Aronson, M. C.; Han, W.-Q. *J. Phys. Chem. C* **2010**, *114*, 14697. (d) Dreyer, A.; Ennen, I.; Koop, T.; Hütten, A.; Jutzi, P. *Small* **2011**, *7*, 3075. (e) Chou, N. H.; Schaak, R. E. *Chem. Mater.* **2008**, *20*, 2081. (f) Hsu, Y.-J.; Lu, S.-Y.; Lin, Y.-F. *Small* **2006**, *2*, 268. (g) Yu, H.; Gibbons, P. C.; Kelton, K. F.; Buhro, W. E. *J. Am. Chem. Soc.* **2001**, *123*, 9198. (h) Chou, N. H.; Schaak, R. E. *J. Am. Chem. Soc.* **2007**, *129*, 7339.

(5) Yarema, M.; Kovalenko, M. V.; Hesser, G.; Talapin, D. V.; Heiss, W. *J. Am. Chem. Soc.* **2010**, *132*, 15158.

(6) Zolotavin, P.; Guyot-Sionnest, P. *ACS Nano* **2010**, *4*, 5599.

(7) Yarema, M.; et al. *ACS Nano* **2012**, *6*, 4113.

(8) Margeat, O.; Amiens, C.; Chaudret, B.; Lecante, P.; Benfield, R. E. *Chem. Mater.* **2005**, *17*, 107.

(9) Dumestre, F.; Chaudret, B.; Amiens, C.; Renaud, P.; Fejes, P. *Science* **2004**, *303*, 821.

(10) Ciuculescu, D.; et al. *Chem. Mater.* **2007**, *19*, 4624.

(11) Desvaux, C.; Amiens, C.; Fejes, P.; Renaud, P.; Respaud, M.; Lecante, P.; Snoeck, E.; Chaudret, B. *Nat. Mater.* **2005**, *4*, 750.

(12) Kovalenko, M. V.; Heiss, W.; Shevchenko, E. V.; Lee, J. S.; Schwinghammer, H.; Alivisatos, A. P.; Talapin, D. V. *J. Am. Chem. Soc.* **2007**, *129*, 11354.

(13) Yarema, M.; et al. *ACS Nano* **2011**, *5*, 3758.

(14) Wołcyrz, M.; Kubiak, R.; Maciejewski, S. *Phys. Status Solidi B* **1981**, *107*, 245.

(15) Cossement, C.; Darville, J.; Gilles, J. M.; Nagy, J. B.; Fernandez, C.; Amoureux, J. P. *Magn. Reson. Chem.* **1992**, *30*, 263.

(16) Indris, S.; et al. *J. Phys. Chem. C* **2011**, *115*, 6433.

(17) Nag, A.; Kovalenko, M. V.; Lee, J.-S.; Liu, W.; Spokoyny, B.; Talapin, D. V. *J. Am. Chem. Soc.* **2011**, *133*, 10612.

(18) (a) Takahashi, H.; Meshitsuka, S.; Higasi, K. *Spectrochim. Acta, Part A* **1975**, *31*, 1617. (b) Adler, H. H.; Kerr, P. F. *Am. Mineral.* **1965**, *50*, 132.

(19) Courtney, I. A.; Dahn, J. R. *J. Electrochem. Soc.* **1997**, *144*, 2045.

(20) Li, J.; Lewis, R. B.; Dahn, J. R. *Electrochem. Solid-State Lett.* **2007**, *10*, A17.

(21) Park, M.-S.; Wang, G.-X.; Kang, Y.-M.; Wexler, D.; Dou, S.-X.; Liu, H.-K. *Angew. Chem., Int. Ed.* **2007**, *46*, 750.

(22) (a) Li, N. C.; Martin, C. R. *J. Electrochem. Soc.* **2001**, *148*, A164. (b) Yu, Y.; Gu, L.; Wang, C.; Dhanabalan, A.; van Aken, P. A.; Maier, J. *Angew. Chem., Int. Ed.* **2009**, *48*, 6485.

(23) Chockla, A. M.; Bogart, T. D.; Hessel, C. M.; Klavetter, K. C.; Mullins, C. B.; Korgel, B. A. *J. Phys. Chem. C* **2012**, *116*, 18079.